Chemical Science

EDGE ARTICLE

View Article Online
View Journal | View Issue



Cite this: *Chem. Sci.*, 2017, **8**, 3566

# Imposing high-symmetry and tuneable geometry on lanthanide centres with chelating Pt and Pd metalloligands†

Mikkel A. Sørensen,[a] Høgni Weihe,[a] Morten G. Vinum,[a] Jesper S. Mortensen,[a] Linda H. Doerrer[b] and Jesper Bendix*[a]

Received 11th January 2017
Accepted 28th February 2017

DOI: 10.1039/c7sc00135e

rsc.li/chemical-science

Exploitation of HSAB preferences allows for high-yield, one-pot syntheses of lanthanide complexes chelated by two Pd or Pt metalloligands, $[M^{II}(SAc)_4]^{2-}$ ($SAc^-$ = thioacetate, M = Pd, Pt). The resulting complexes with 8 oxygen donors surrounding the lanthanides can be isolated in crystallographically tetragonal environments as either $[NEt_4]^+$ (space group: *P*4/*mcc*) or $[PPh_4]^+$ (space group: *P*4/*n*) salts. In the case of M = Pt, the complete series of lanthanide complexes has been structurally characterized as the $[NEt_4]^+$ salts (except for Ln = Pm), while the $[PPh_4]^+$ salts have been structurally characterized for Ln = Gd–Er, Y. For M = Pd, selected lanthanide complexes have been structurally characterized as both salts. The only significant structural difference between salts of the two counter ions is the resulting twist angle connecting tetragonal prismatic and tetragonal anti-prismatic configurations, with the $[PPh_4]^+$ salts approaching ideal $D_{4d}$ symmetry very closely ($\varphi$ = 44.52–44.61°) while the $[NEt_4]^+$ salts exhibit intermediate twist angles in the interval $\varphi$ = 17.28–27.41°, the twist increasing as the complete 4f series is traversed. Static magnetic properties for the latter half of the lanthanide series are found to agree well in the high temperature limit with the expected Curie behavior. Perpendicular and parallel mode EPR spectroscopy on randomly oriented powder samples and single crystals of the Gd complexes with respectively Pd- and Pt-based metalloligands demonstrate the nature of the platinum metal to strongly affect the spectra. Consistent parametrization of all of the EPR spectra reveals the main difference to stem from a large difference in the magnitude of the leading axial term, $B_2^0$, this being almost four times larger for the Pt-based complexes as compared to the Pd analogues, indicating a direct $Pt(5d_{z^2})$–Ln interaction and an arguable coordination number of 10 rather than 8. The parametrization of the EPR spectra also confirms that off-diagonal operators are associated with non-zero parameters for the $[NEt_4]^+$ salts, while only contributing minimally for the $[PPh_4]^+$ salts in which lanthanide coordination approximates $D_{4d}$ point group symmetry closely.

## Introduction

During the last decade and a half, the interest in the coordination chemistry of the lanthanides has been refuelled by the prosperity of mono- and polynuclear 4f metal complexes in the field of molecular magnetism. Polynuclear clusters and extended networks based on especially gadolinium(III) have shown large magnetocaloric effects,[1–3] rendering these complexes potentially applicable in low temperature magnetic cooling.[4] On the other hand, low nuclearity complexes of anisotropic lanthanide ions have been found to behave as single-molecule magnets with properties superior to those of the archetypal 3d metal clusters of the 1990s.[5–8] Notably, complexes containing a single lanthanide ion, so-called single-ion magnets,[9] have exhibited remarkably slow spin-lattice relaxation,[10–14] with relaxation times reaching up to several 1000 s at liquid helium temperatures.[15] These long relaxation times are considered a consequence of relaxation *via* excited states (Orbach relaxation) within the ground Russell-Saunders (RS) multiplet, which is split by the crystal field experienced by the 4f ion.[16,17] Therefore, the optimization of crystal field splittings by appropriate tailoring of ligand environments has been a key preparative target.[18] However, despite the achievement of large crystal field splittings, quantum tunnelling of the magnetization (QTM) within the ground state often dominates the low temperature spin relaxation, limiting the timescale of the relaxation events to the order of milliseconds.[13,19–21]

[a]*Department of Chemistry, University of Copenhagen, Universitetsparken 5, DK-2100 Copenhagen, Denmark. E-mail: bendix@kiku.dk*

[b]*Department of Chemistry, Boston University, 590 Commonwealth Avenue, Boston, Massachusetts 02215, USA*

† Electronic supplementary information (ESI) available: Synthetic procedures, crystallographic details, additional magnetic data, experimental details on EPR measurements. CCDC 1526314–1526340. For ESI and crystallographic data in CIF or other electronic format see DOI: 10.1039/c7sc00135e

Therefore, design criteria for obtaining pure crystal field states have also been suggested.[22] Low symmetry components of the crystal field serve as to connect the different substates within the ground RS multiplet, thereby increasing tunnelling probabilities causing unwanted, fast spin relaxation. Consequently, the design criteria aimed at maximizing crystal field state purity evolve around tuning of the point group symmetry of the crystal field. The recent dawn of mononuclear lanthanide complexes as molecular spin qubits[23,24] adds to the interest in tailoring electronic structures and chemical functionalities allowing for implementation in devices *e.g.* through surface attachment. All suggested criteria guide the synthetic chemist towards the rational design and control of the crystal field environment and ligand periphery, and in principle, this seems straightforward.

Alas, the structural design of lanthanide complexes is less simple than for *n*d metal complexes for various reasons. Firstly, the high coordination number characteristic of the lanthanides complicates control of the environment if only simple ligands of low denticity are employed. This can either be overcome by using bulky ligands, thereby lowering coordination numbers,[25–30] or by coordinatively saturating the metal ion by employing a single[31–34] or only few[35–38] ligands of high denticity. Secondly, the lack of ligand field stabilization energies renders coordination geometries less predictable and consequently specific symmetries are more easily imposed through the choice of ligand.

The platinum(II) complexes $[Pt^{II}(SC(O)R)_4]^{2-}$ (R = Me (thioacetate), Ph (thiobenzoate)) have previously been reported on their own (for R = Me),[39] and as constituent units of a family of heterobimetallic lantern complexes of formulation $[Pt^{II}M^{II}(SC(O)R)_4(solv)_n]$ (M = Mg, Ca, Fe, Co, Ni, Zn; solv = solvent molecules),[39–42] $A[Pt^{II}M^{II}(SC(O)Me)_4(NCS)]$ (A = [Na(15-crown-5)], $[Na(12\text{-crown-4})_2]$; M = Mn, Co, Ni, Zn),[43] and $[Pt^{II}Cr^{III}(SC(O)Ph)_4(NCS)]_n$.[43] In the bimetallic lantern compounds, the soft Lewis acidity of platinum(II) allows for selective coordination by the soft sulphur donors, while the harder Lewis acids, that is the divalent *n*s and 3d metal ions, are selectively coordinated by the oxygen atoms of the thiocarboxylates. This design concept relying on the hard–soft acid–base (HSAB) principle should be expandable to encompass the even harder Lewis acids such as the trivalent lanthanide ions. Herein, we report such an expansion, using the platinum metal complexes $[M^{II}(SAc)_4]^{2-}$ ($SAc^-$ = thioacetate, M = Pd, Pt) as chelating tetradentate metalloligands. The predictable square-planar geometry of the platinum metal complex facilitates tetragonal symmetry of the resulting $[Ln^{III}\{M^{II}(SAc)_4\}_2]^-$ complexes, and by selecting appropriate counter cations ($[NEt_4]^+$ (for M = Pt: **1Ln**, for M = Pd: **1Ln′**), $[N^nPr_4]^+$, or $[PPh_4]^+$ (for M = Pt: **2Ln**, for M = Pd: **2Ln′**)), the tetragonal symmetry can be crystallographically imposed in the solid state. We describe the synthesis as well as the structural, static magnetic, and EPR spectroscopic characterizations of this new family of high-symmetry lanthanide complexes.

## Results and discussion

The reaction of thioacetate as its potassium salt with $K_2[PtCl_4]$ and hydrated trivalent lanthanide chlorides in aqueous solution cleanly yielded the anionic complexes $[Ln\{Pt(SAc)_4\}_2]^-$, which could be isolated as either the $[NEt_4]^+$ or $[N^nPr_4]^+$ salts in the presence of an excess of these cations (Scheme 1). This yielded $[NEt_4][Ln\{Pt(SAc)_4\}_2]$ (**1Ln**) as golden quadratic plate-shaped single crystals, while near-amorphous powders (as verified by PXRD, not shown) of $[N^nPr_4][Ln\{Pt(SAc)_4\}_2]$ were obtained (see ESI† for synthetic details). It proved possible to synthesize the **1Ln** salts (*i.e.* the $[NEt_4]^+$ salts) for all lanthanides (excluding promethium) as well as yttrium by appropriately adjusting the synthetic protocol. The isomorphism of the **1Ln** compounds was confirmed by single crystal X-ray diffraction. The crystallographic details and structure of **1Gd** are given in Table 1 and Fig. 1, respectively. The crystallographic details for the remainder of the **1Ln** compounds are collected in Tables S1–S4 of the ESI.†

In the preparation of **1Ln** for the full lanthanide series, it was found necessary to modify the employed protocol significantly when moving from the earlier to the later lanthanides. The reactions for especially the earliest lanthanides (La, Ce) had to be carried out at very dilute conditions in order to obtain crystals of a size suitable for structure determination. Upon moving across the series, the concentration of the reaction mixture had to be gradually increased in order to obtain satisfactory yields. For the last four lanthanides, the decrease in the solvent volume rendered the method used for preparing the remainder of the **1Ln** complexes inconvenient. Instead, a concentrated solution of the metalloligand was prepared by briefly heating a concentrated aqueous solution of KSAc and $K_2[PtCl_4]$. Addition of the relevant lanthanide chloride to this solution resulted in the development of some turbidity, the turbidity being more pronounced the later the lanthanide. For **1Er**, **1Tm**, and **1Yb** the turbidity completely disappeared in the presence of a large excess of $[NEt_4]Cl$, and subsequent gentle heating initiated the

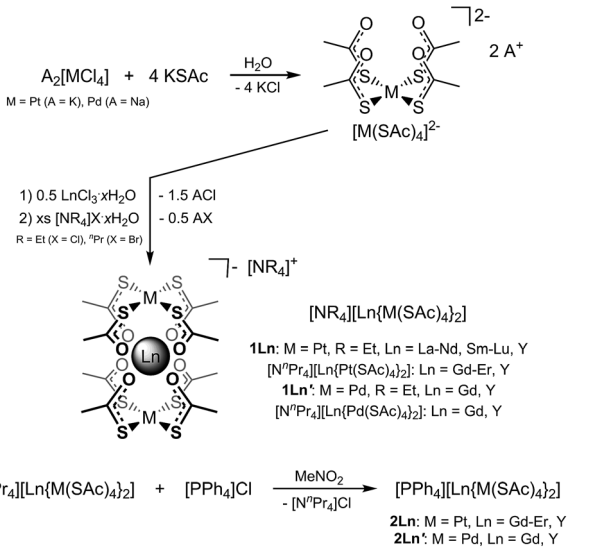


Scheme 1 Synthesis of **1Ln**, $[N^nPr_4][Ln\{Pt(SAc)_4\}_2]$, and **2Ln** from the dianionic platinum metalloligand $[Pt^{II}(SAc)_4]^{2-}$ ($SAc^-$ = thioacetate), and of **1Ln′**, $[N^nPr_4][Ln\{Pd(SAc)_4\}_2]$, and **2Ln′** from the analogous palladium-based ligand.

Table 1 Crystallographic data and refinement parameters for **1Gd** and **2Gd**

| | **1Gd** | **2Gd** |
|---|---|---|
| Formula | $C_{24}H_{44}GdNO_8Pt_2S_8$ | $C_{40}H_{44}GdO_8PPt_2S_8$ |
| $M_r$ | 1278.56 | 1487.70 |
| $T$/K | 122(1) | 123(1) |
| Crystal system | Tetragonal | |
| Space group | $P4/mcc$ (no. 124) | $P4/n$ (no. 85) |
| $a$/Å | 8.6134(3) | 12.6662(5) |
| $c$/Å | 25.4434(9) | 15.1584(6) |
| $V$/Å$^3$ | 1887.66(11) | 2431.90(17) |
| $Z$ | 2 | 2 |
| $\rho_{calc}$/g cm$^{-3}$ | 2.2493 | 2.0315 |
| $\mu$/mm$^{-1}$ | 9.612 | 7.508 |
| $F_{000}$ | 1214 | 1422 |
| Crystal size/mm$^3$ | 0.10 × 0.10 × 0.040 | 0.12 × 0.12 × 0.080 |
| Radiation | Mo Kα ($\lambda$ = 0.71703 Å) | |
| 2$\theta$ range/° | 4.72–57.4 | 4.54–57.38 |
| Reflections collected | 31 200 | 48 108 |
| Independent reflections | 1263 | 3157 |
| $R_{int}$, $R_\sigma$ | 0.0334, 0.0107 | 0.0510, 0.0199 |
| Param/restraints | 91/3 | 139/0 |
| $S$ (on $F^2$) | 1.089 | 1.054 |
| $R_1$, w$R_2$($I \geq 2\sigma(I)$) | 0.0164, 0.0522 | 0.0175, 0.0351 |
| $R_1$, w$R_2$ (all data) | 0.0215, 0.0559 | 0.0248, 0.0375 |
| $\Delta\rho_{max}/\Delta\rho_{min}$/e Å$^{-3}$ | 1.43/−0.90 | 2.46/−0.81 |

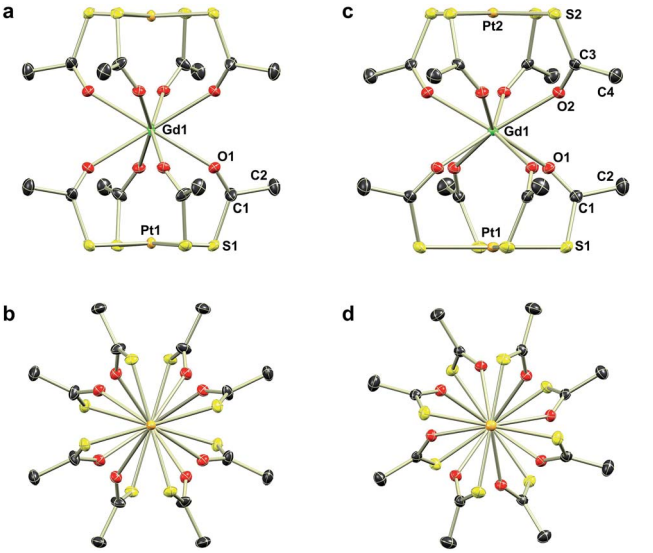


Fig. 1 Thermal ellipsoids plots (50% probability) of the complex anions in the structures of **1Gd** (a and b) and **2Gd** (c and d) viewed perpendicular to (a and c) and along (b and d) the four-fold axis. For **1Gd** only one of the two equally occupied disordered parts of the thioacetate is shown. The oxygen and sulphur atoms belonging to the omitted part are labelled O1a and S1a, respectively. Hydrogen atoms are omitted for clarity. Colour code: Gd, green; Pt, orange; O, red; S, yellow; C, dark grey. Selected bond distances and angles: **1Gd**, Gd1–O1 2.443(3) Å; Gd1–O1a 2.355(3) Å; Pt1–S1 2.310(3) Å; Pt1–S1a 2.311(3) Å; S1–Pt1–S1 175.74(16)°; S1a–Pt1–S1a 178.13(16)°; **2Gd**, Gd1–O1 2.3833(15) Å; Gd1–O2 2.4010(15) Å; Pt1–S1 2.3219(6) Å; Pt2–S2 2.3180(6) Å; S1–Pt1–S1 178.65(2)°; S2–Pt2–S2 179.88(3)°.

formation of square-shaped golden crystals. Also for this procedure, satisfactory yields required much higher concentrations for the latest lanthanides. Addition of solid $LuCl_3 \cdot 6H_2O$ to a concentrated solution of the metalloligand resulted in a considerable amount of precipitate rather than the turbidity observed for the larger predecessors. Treatment with excess $[NEt_4]Cl$ did not fully redissolve the solid, and despite the remaining solids being filtered off prior to crystallization of the product, **1Lu** invariably contained a minor impurity as judged from CHNS elemental analysis and PXRD (see ESI†).

The $[N^nPr_4][Ln\{Pt(SAc)_4\}_2]$ salts are less easily precipitated than the analogous $[NEt_4]^+$ salts (**1Ln**), and consequently the protocol used for the synthesis of the **1Ln** compounds for the four latest lanthanides was adapted. Recrystallization of the crude $[N^nPr_4][Ln\{Pt(SAc)_4\}_2]$ products by slow evaporation of a concentrated acetone solution at room temperature yielded single crystals. Structure determination was however impeded by an inherently high mosaicity of the so-obtained crystals.

Direct addition of $[PPh_4]Cl$ to aqueous solutions containing $[Ln\{Pt(SAc)_4\}_2]^-$ precipitates the non-coordinated metalloligand as golden-yellow crystals of formulation $[PPh_4]_2[Pt(SAc)_4] \cdot 4.5H_2O$,[39] preventing direct preparation of the $[PPh_4]^+$ salts. However, facilitated by the reasonable solubility of the near-amorphous crude $[N^nPr_4][Ln\{Pt(SAc)_4\}_2]$ salts in polar organic solvents like acetonitrile, nitromethane, and acetone, golden quadratic single crystals of $[PPh_4][Ln\{Pt(SAc)_4\}_2]$ (**2Ln**) could instead be obtained in high yields by the metathesis reaction of crude $[N^nPr_4][Ln\{Pt(SAc)_4\}_2]$ and $[PPh_4]Cl$ in $MeNO_2$ (Scheme 1).

Single crystal X-ray diffraction revealed the synthesized **2Ln** compounds to be isostructural. The crystallographic details and structure of **2Gd** are given in Table 1 and Fig. 1, respectively. The crystallographic details of the remaining **2Ln** compounds are given in Tables S5 and S6 of the ESI.†

Single crystal X-ray diffraction revealed the tetraethylammonium salts (**1Ln**) to be isomorphous, a result that was corroborated by PXRD (Fig. S1–S3, ESI†). Due to their isomorphism, the structures of **1Ln** will be discussed in comparison to that of **1Gd**. The structure solution revealed the coordination of two $[Pt(SAc)_4]^{2-}$ complexes to the gadolinium ion through the available oxygen atoms of the thiocarboxylates, yielding an eight-coordinate $Gd^{III}$ centre. The complex can thus be described as the homoleptic metalloligand complex of gadolinium(III) crystallized with one tetraethylammonium counter ion. The salt crystallized in the centrosymmetric tetragonal space group $P4/mcc$ with two formula units in the unit cell. The Gd1, Pt1, and the nitrogen atom of the counter ion (N1) all occupy special positions of four-fold site symmetry, and consequently the asymmetric unit contains only one eighth of a formula unit. As described in the ESI,† the single thioacetate contained in the asymmetric unit is disordered over two positions, the two fragments being equally occupied. A structure determination for **1Gd** at room temperature (Table S4, ESI†) revealed an identical disorder (Fig. S4, ESI†), suggesting it to be static in nature. This was corroborated by the electron density map in the region of the oxygen atom positions, showing a clear

peanut-shaped electron density rather than an oblate one, indicating two closely spaced but localized positions of the disordered oxygen atom. The oxygen and sulphur atoms belonging to the part of the thioacetate that is omitted in Fig. 1 are labelled with an "a"-extension. Each platinum centre is coordinated by four thioacetates through the sulphur atoms resulting in a square planar geometry, as expected for the $5d^8$ ion. The planes spanned by either the four S1 or the four S1a atoms are perpendicular to the four-fold axis by symmetry. The platinum atom is shifted slightly out of plane either towards (for the $S1_4$ plane) or away from (for the $S1a_4$ plane) the gadolinium centre by 0.086 Å and 0.038 Å, respectively. These out of plane shifts are slightly larger than those observed in the related heterobimetallic lantern complexes,[39–43] and significantly larger than for the non-coordinated metalloligand in which the platinum sits exactly in the $S_4$ plane.[39]

Thiocarboxylates as ligands for lanthanides are uncommon, and to this date only two structurally characterized examples have been reported.[44,45] In both these cases, the thiocarboxylates act as chelating bidentate ligands, and the bridging of a lanthanide ion and a transition metal in the $\mu_{1,3}$-fashion observed for **1Gd** is hitherto unknown. A related bridging motif is however observed for a series of heterobimetallic dithiooxalate-bridged compounds of formulation $[\{Ln^{III}(H_2O)_n\}_2\{Ni^{II}(dto)_2\}_3]\cdot xH_2O$ ($dto^{2-}$ = dithiooxalate)[46–48] as well as for the systems $[M^{III}\{(dto)Dy^{III}(tp)_2\}_3]\cdot 4MeCN\cdot 2CH_2Cl_2$ ($M^{III}$ = $Fe^{III}$, $Co^{III}$; $tp^-$ = hydrotrispyrazolylborate),[49] in which the dithiooxalate ligands selectively coordinate the softer 3d metal ions through the sulphur atoms, while the lanthanide ions are exclusively coordinated by the oxygen atoms of the bridging ligands.

In the evaluation of the nature of the crystal field experienced by the lanthanide ion in the **1Ln** salts, two angles are of relevance. Firstly, the compression angle, $\theta$ (Fig. 2), defined as the angle between the four-fold axis and the Ln–O bond, describes the axial distortion of the coordination environment. The cube-value of $\theta = \cos^{-1}(1/\sqrt{3}) \approx 54.7°$ (*i.e.* half the tetrahedral angle) constitutes the non-compressed scenario, while smaller and larger angles correspond to elongation and compression, respectively. The angle, $\varphi$, between the diagonals of the two squares constituted by the two sets of oxygen donor atoms, is illustrated in Fig. 2. This twist angle, also referred to as the skew angle,[5,50] is key for determining the point group symmetry at the lanthanide site, which in turn is crucial for appropriately describing the crystal field substate composition of lanthanide complexes. In the case of an axial distortion of the crystal field environment (*i.e.* for $\theta \neq 54.7°$), the position of the lanthanide ion belongs to the $D_{4h}$ and $D_{4d}$ point groups for the two extremes $\varphi = 0°$ (square prism) and 45° (square antiprism), respectively.

The $\theta$ and $\varphi$ angles were evaluated for the entire **1Ln** series and are given in the upper and lower panels of Fig. 3, respectively (excluding **1Y**). As a result of the disorder in the thioacetates, two different crystal field environments exist in the crystal, defined by a single type of oxygen atoms (O1 or O1a) for symmetry reasons. As the disorder is 50 : 50, so is the distribution between the two crystal field environments. From Fig. 3 it is evident how both angles depend on the lanthanide ion, *i.e.* the ionic radii. A smooth decrease in the degree of axial compression is observed following the decrease in ionic radius upon going from **1La** to **1Lu**, the $\theta$ values varying between 62.73° (**1La**, O1a) and 58.87° (**1Lu**, O1). The difference in degree of axial compression between the two different crystal field environments is on the order of a few degrees for all **1Ln** derivatives, the maximum difference being that for **1Gd**, in which $\theta_{O1a} - \theta_{O1} = 2.84°$. The value of $\varphi$ smoothly increases upon going from **1La** to **1Lu**, the smallest value being 17.28° for the O1 environment in **1La**, and the largest 27.41° for the O1a environment in **1Lu**. The difference in the value of the angle for the two different environments for a specific lanthanide is generally small, and never exceeds 1.5°.

Despite the highlighted differences, the two crystal field environments found in the crystals of **1Ln** are identical from a symmetry point of view. As the twist angles are in between the two extremes of $\varphi = 0°$ and 45°, the point group symmetry of the lanthanide site lowers to $D_4$ ($C_4$ with disorder, *cf.* ESI†)

In the crystal packing of **1Gd** (Fig. S5, ESI†) all complexes have their Pt–Gd–Pt axis parallel to the *c*-axis of the unit cell, with the lanthanide complexes being arranged end-to-end along this direction. The shortest Gd···Gd distance equals the length

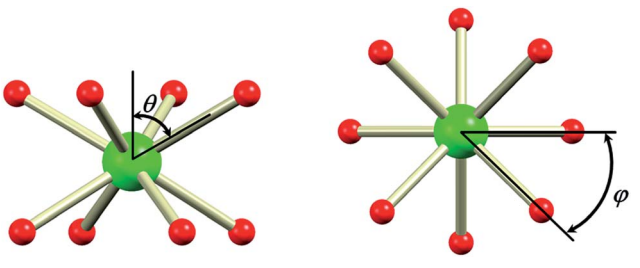


Fig. 2 The compression angle, $\theta$, between the four-fold axis and the Ln–O bond (left), and the twist angle, $\varphi$, between the diagonals of the two squares constituted by the two sets of four oxygen donor atoms above and below the lanthanide ion, when viewed along the four-fold axis (right).

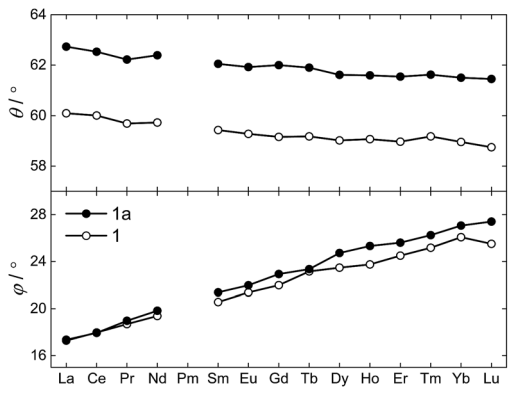


Fig. 3 The compression angle $\theta$ (top), and the twist angle $\varphi$ (bottom), for **1Ln** at $T = 122(1)$ K as function of the lanthanide, determined from the X-ray single crystal structures. 1 and 1a refer to the values related to the crystal field environments defined by the O1 and O1a atoms, respectively.

of the *a*-axis (or *b*-axis) of the unit cell of 8.6134(3) Å. Along the *c*-axis the shortest Gd···Gd distance is half the length of the axis, 12.7217(5) Å. The packing of the cations and anions is CsCl-like with each ion having eight nearest neighbours of the opposite kind.

The shortest intermolecular Pt···Pt distance of 5.3240(4) Å rules out any metallophillic Pt···Pt interactions similar to those observed for the related heterobimetallic lantern complexes.[40,41] Likely, the charge on the complexes and the packing with the counter ions both contribute to suppress Pt···Pt interactions. However, the fact that metallophillic interactions have been observed in some of the anionic lantern complexes of the divalent 3d metals,[43] points to packing effects involving the counter ions as the main reason. It is conceivable that if the need for the counter ion could be circumvented, *e.g.* using mixed complexes with an isoelectronic $Au^{III}$-based metalloligand, such di- or oligomerization can regain importance.

The synthesis and structural characterization of a full series of isomorphous lanthanide complexes is not a matter of course. Rather, the lanthanide contraction amounting to a ~15% reduction in ionic radii for the trivalent ions, commonly leads to structural discontinuities across the 4f series. Here, the polydentate, yet flexible nature of the employed metalloligands facilitate the non-trivial preparation of all members of the **1Ln** family (with the obvious exception of **1Pm**) and hence allows for a detailed study of the full series of lanthanide ions in an identical crystal field environment. Evaluation of the unit cell parameters for the **1Ln** complexes determined from single-crystal X-ray diffraction at $T = 122$ K (Fig. 4) reveals the length of the *a*-axis and the unit cell volume to conform to the expected trend. The length of the *c*-axis is found to increase upon reducing the size of the lanthanide ion. Albeit counterintuitive, this lengthening of the *c*-axis can however also be understood as a result of the lanthanide contraction (a detailed argument for this is presented in the ESI†).

Switching to the salts with tetraphenylphosphonium counter ions (**2Ln**), the synthesized members of this series were also found to be isostructural from single crystal X-ray diffraction experiments, and this was confirmed by PXRD (Fig. S6, ESI†). Consequently, the description of their structures will take its starting point at the gadolinium derivative. **2Gd** crystallized in the centrosymmetric tetragonal space group $P4/n$ with two formula units in the unit cell. The Gd1, Pt1, and Pt2 atoms along with the phosphorus atom belonging to the tetraphenylphosphonium ion all occupy special positions of four-fold site symmetry. As a result of the high symmetry, only a quarter formula unit is contained in the asymmetric unit. As opposed to the structures of the tetraethylammomium salts (**1Ln**), no disorder of the thioacetates was observed in the structures of **2Ln**. The structural characteristics of the complex anion discussed for **1Gd** also apply to **2Gd**. However, one very important difference between the two salts is observed when evaluating the values of the twist angle $\varphi$. The increase of ~10° in this parameter value for **1Ln** observed upon traversing the f-block was discussed above. For those lanthanides for which the analogous **2Ln** compounds were prepared, the span of $\varphi$ angles is from 21.99°/22.94° for **1Gd** to 24.50°/25.61° for **1Er**. For the tetraphenylphosphonium salts (**2Ln**) of the same central ions, $\varphi$ shows a variation as small as 0.09° (44.52–44.61°), much less than the approximately 2.5° variation seen for the analogous **1Ln** salts. The pronounced structural invariance observed for the **2Ln** can be understood when examining the packing of neighbouring cations and anions in the crystal as illustrated for **2Gd** in Fig. 5 (the crystal packing of **2Gd** is given in Fig. S7, ESI†). The space-filling model highlights how a phenyl group from the tetraphenylphosphonium ion occupies the void space in between neighbouring thioacetates that are 90° apart around the four-fold axis. By symmetry, all void spaces in between neighbouring $CH_3C(O)S^-$-groups are occupied by phenyl groups. While this on its own does not enforce a twist angle of 45°, it seems reasonable to assume that this particular conformation of two metalloligands with respect to each other facilitates the most efficient accommodation of the eight phenyl moieties. The twist angle of ~45° results in excellent approximation to $D_{4d}$ point group symmetry (which cannot be strictly imposed crystallographically) at the lanthanide site. This is of crucial importance for the description of the electronic structure of these systems, as evidenced by the EPR spectra of the gadolinium derivatives (*vide infra*). The crystallographic

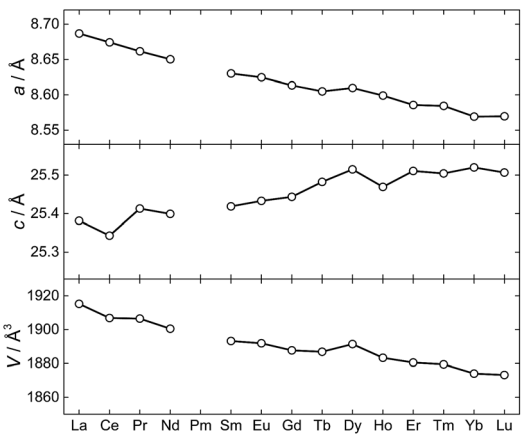


Fig. 4 The unit cell parameters for **1Ln** at $T = 122(1)$ K determined from the X-ray single crystal structures.

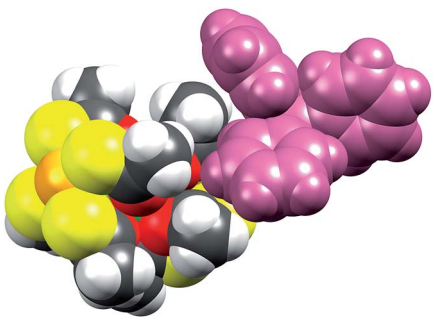

Fig. 5 Space-filling model of **2Gd** showing how the phenyl group from the tetraphenylphosphonium counter ion occupies the void space in between two neighbouring thioacetates. Colour code: Gd, green; Pt, orange; O, red; S, yellow; C, dark grey; H, light grey. The entire tetraphenylphosphonium ion is coloured purple for clarity.

inequivalence of the oxygen atoms O1 and O2 (Fig. 1c) results in two slightly different values of $\theta$. For **2Gd**, the angle amounts to 60.03° or 61.23° depending on the oxygen atom chosen as reference. The average of these values, 60.63°, is within uncertainties identical to the average value of $\theta$ for the two different crystal field environments found for **1Gd** of 60.58°. As for the **1Ln** systems, the lanthanide centres in **2Ln** are also well separated with nearest neighbour distances of *ca.* 9.8 Å.

When examining Fig. 5, the build-in soft functionality terminating the lanthanide complexes is immediately evident. The affinity of not only the sulphur atoms but also the platinum centre for soft metal centres (*i.e.* another platinum centre) has been firmly demonstrated by strong metallophillic interactions in the heterobimetallic complexes already discussed.[40–42] The planar nature of the $PtS_4$ units, in principle, renders these extremely well-suited for deposition on softer substrates like gold.

With the prospect of tuning surface interaction strengths and demonstrating the generalizable nature of the chemistry presented here, we synthesized the gadolinium and yttrium derivatives with palladium(II) substituting for platinum(II), giving rise to $[NEt_4][Ln\{Pd(SAc)_4\}_2]$ (**1Ln′**), $[N^nPr_4][Ln\{Pd(SAc)_4\}_2]$, and $[PPh_4][Ln\{Pd(SAc)_4\}_2]$ (**2Ln′**) with Ln = Gd, Y (see ESI† for synthetic details). The obtained compounds were found to be strictly isostructural with their platinum counterparts (crystallographic data are given in Table S7, ESI†), as evidenced by the structural overlays of the Gd derivatives shown in Fig. 6. Despite their strictly isostructural nature, a few important adjustments were necessary in their preparations. Under reaction conditions employed in the synthesis of the platinum systems, sulphide formation seemed to pose a problem for the preparation of the palladium complexes. This was however avoided by constantly keeping thioacetate in excess. The greater lability of palladium over platinum allowed for a shortening of reaction times, and the $[NEt_4][Ln\{Pd(SAc)_4\}_2]$ (**1Ln′**) and $[N^nPr_4][Ln\{Pd(SAc)_4\}_2]$ salts could consequently be precipitated immediately after complete addition of all starting materials to the reaction mixture. The palladium derived complexes are intensely yellow in colour compared to the light golden yellow nature of the platinum based systems. The pronounced difference in the strength of the interaction between the lanthanide ion and the group 10 metal (*vide infra*), is sufficiently large to possibly influence the optical properties and lead to differences between the platinum and palladium derivatives of the luminescent lanthanide ions.

The crystalline purity and isomorphism of the palladium derivatives was confirmed by PXRD (Fig. S8, ESI†). We note that **1Ln′** and **2Ln′** are the first structurally characterized species containing mono-thiocarboxylates coordinated to palladium.

The molar magnetic susceptibilities of the compounds **1Ln** (Ln = Gd–Yb) and **2Ln** (Ln = Gd–Er) were investigated in an applied magnetic field of $B$ = 100 mT. The temperature dependence of the $\chi_M T$ products is given in Fig. 7. The high temperature values of the $\chi_M T$ products are generally in good agreement with the expected Curie constants (Table S8, ESI†). For all compounds but **1Gd** and **2Gd**, the value of $\chi_M T$ decreases upon lowering the temperature, as a result of the depopulation of $m_J$ substates within the crystal field split ground $J$ manifold. In general, the powder-averaged susceptibilities and magnetization data (Fig. S9–S15, ESI†) are highly similar when comparing the **1Ln** and **2Ln** salts. This suggests that whilst the composition of the crystal field states might change significantly upon changing the point group symmetry, the relative energies of the states, and hence the total splitting of the manifold, might be less affected. The plausibility of this is supported by the on-average negligible difference in $\theta$ between the two different salts for a given lanthanide, as the axial crystal field parameters are strongly dependent on this parameter but show only slight or no dependence on $\varphi$.[22] The non-superimposable reduced magnetization isotherms (Fig. S9–S15, ESI†) observed for all compounds but **1Gd** and **2Gd** indicate the presence of significant anisotropy, low-lying excited states or a combination of the two. For **1Gd** and **2Gd** a collective fit of the $\chi_M T(T)$ and reduced magnetization data to an isotropic Zeeman Hamiltonian resulted in isotropic $g$-values of 1.98(3) and 2.03(3) for **1Gd** and **2Gd**, respectively. Both these values are within error of the expected 2.00.

In order to investigate the importance of the difference in point group symmetry further and probe a possible effect of the Pd/Pt metal centre on the electronic structure of the lanthanide, powder X-band electronic paramagnetic resonance (EPR)

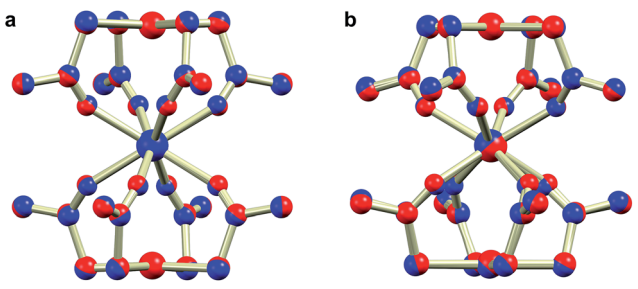


Fig. 6 Ball and stick representations of structural overlays of room temperature crystal structures of **1Gd** and **1Gd′** (a), and **2Gd** and **2Gd′** (b). The platinum and palladium derivatives are shown in red and blue, respectively.

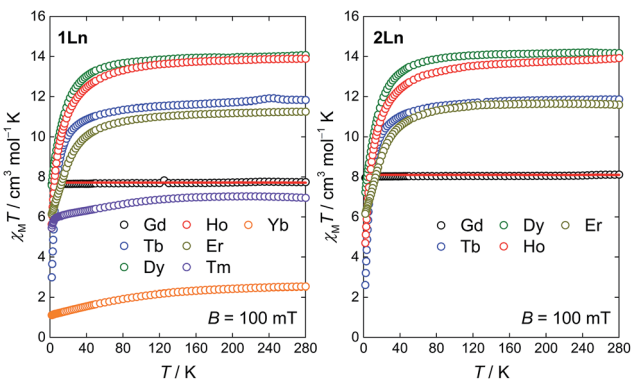


Fig. 7 Temperature dependence of the $\chi_M T$ products for powder samples of **1Ln** (Ln = Gd–Yb, left) and **2Ln** (Ln = Gd–Er, right) recorded in a static magnetic field of $B$ = 100 mT. The red lines represent fits of the gadolinium data to an isotropic Zeeman Hamiltonian.

spectra of the gadolinium derivatives doped into their respective yttrium hosts at a nominal molar concentration of 2% were recorded. The room temperature spectra of the platinum-based complexes **1Gd** and **2Gd** doped into their respective host lattices ($\mathbf{1Y_{0.98}Gd_{0.02}}$ and $\mathbf{2Y_{0.98}Gd_{0.02}}$) recorded with the microwave polarization either perpendicular or parallel to the applied magnetic field are given in the upper panels of Fig. 8 (details on the EPR experiments are given in the ESI†). The structured nature of the spectra calls for the inclusion of crystal field effects, which generate a zero-field splitting of the $S = 7/2$ ground state. Due to the absence of orbital momentum for the gadolinium(III) centre, the splitting arises from the interactions with higher lying Russell-Saunders multiplets, and the effects are therefore small, as the first excited multiplet is placed approximately 30 000 $cm^{-1}$ away from the ground one.[51] The small magnitude of the zero-field splitting of gadolinium(III) makes the frequency characteristic of X-band EPR well-suited for the quantization of said splitting. This contrasts the need for the application of high-field and frequency EPR, which is normally applied for the determination of zero-field splittings in lanthanides with unquenched orbital momentum (*i.e.* $L \neq 0$).[52,53] By considering the minimal, common $C_4$ symmetry of the gadolinium site, the appropriate Hamiltonian following the Stevens approach is[5]

$$\hat{\boldsymbol{H}} = \mu_B B \mathbf{g} \hat{\mathbf{S}} + \sum_{k=2,4,6} B_k^0 \hat{\mathbf{O}}_k^0 + B_4^{+4} \hat{\mathbf{O}}_4^{+4} + B_6^{\pm 4} \hat{\mathbf{O}}_6^{\pm 4} \quad (1)$$

where the first term accounts for the Zeeman effect, and the latter terms for the zero-field splitting of the ground state. In the case of perfect $D_{4d}$ symmetry the two latter zero-field splitting terms vanish,[5] while only the operator associated with the $B_6^{-4}$ parameter does so in the case of $D_{4h}$ symmetry.[54] In the parametrization commonly used for zero-field splittings of *n*d metal ions, the second order axial parameter is denoted *D* rather than $B_2^0$. We note that these are related through $3B_2^0 = D$.[17] Details on the fitting procedure are given in the ESI.†

Best fits to the Hamiltonian (1) were found to provide excellent descriptions of the powder spectra of $\mathbf{1Y_{0.98}Gd_{0.02}}$ and

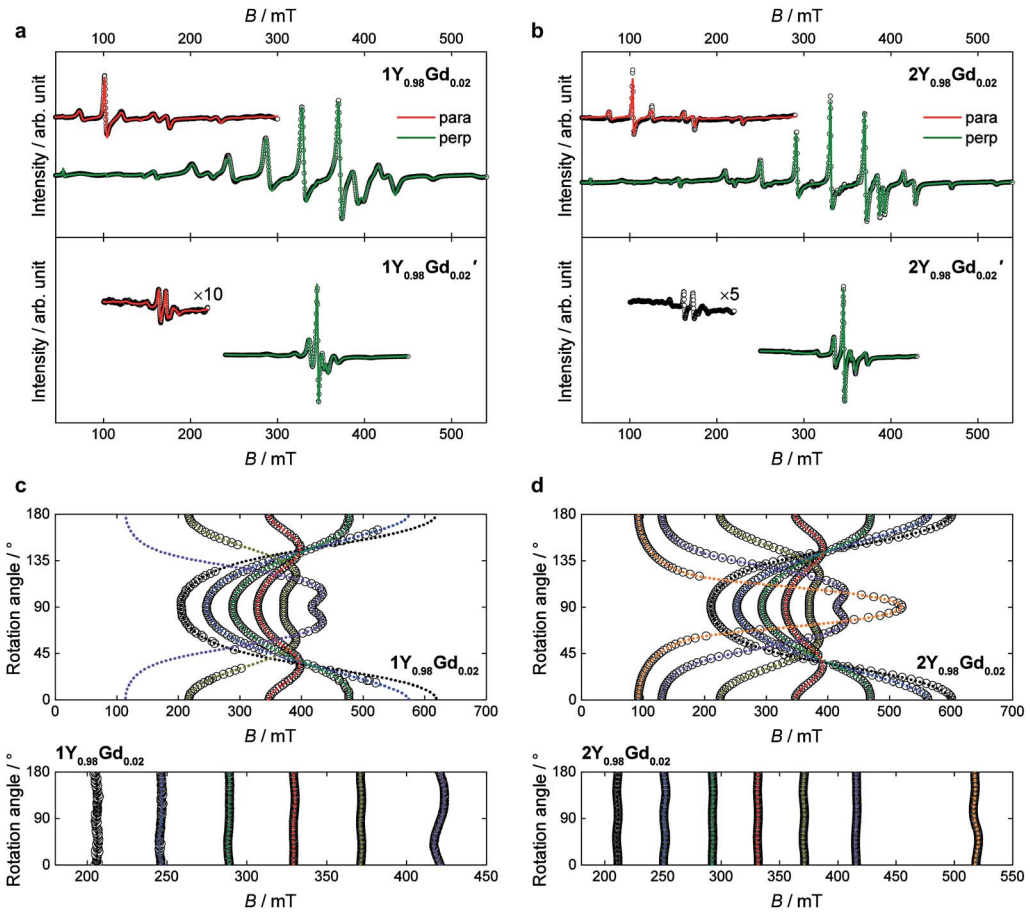


Fig. 8 Room temperature powder and single crystal X-band EPR spectra of $\mathbf{1Y_{0.98}Gd_{0.02}}$ and $\mathbf{1Y_{0.98}Gd_{0.02}}'$ (a and c), and $\mathbf{2Y_{0.98}Gd_{0.02}}$ and $\mathbf{2Y_{0.98}Gd_{0.02}}'$ (b and d). In the powder spectra (a and b), the green and red lines give the best fits of the perpendicular and parallel polarization mode data, respectively. The parallel mode data for $\mathbf{2Y_{0.98}Gd_{0.02}}'$ is too void of features to produce an unambiguous fit. In the single crystal spectra (c and d), the open symbols correspond to the determined line positions at each given angle while the dotted lines correspond to best fits of these positions. In the upper panels the angle of rotation is that between the four-fold axis and the orientation of the magnetic field, so that at 0° the two are parallel. In the lower panels, the rotation is in the *xy*-plane, the zero-point being arbitrarily defined. For $\mathbf{1Y_{0.98}Gd_{0.02}}$, the seventh resonance line (the line at highest field in the *xy*-rotation spectra), has too little intensity for its position to be reliably determined.

$\mathbf{2Y_{0.98}Gd_{0.02}}$ for both polarization modes. Despite the 50 : 50 disorder in the crystal field, characteristic of the **1Ln** compounds, it was possible to describe the spectra of $\mathbf{1Y_{0.98}Gd_{0.02}}$, assuming a single gadolinium site in $C_4$ symmetry. The only manifestation of said disorder is the greater linewidth of the resonance lines for $\mathbf{1Y_{0.98}Gd_{0.02}}$ over those for $\mathbf{2Y_{0.98}Gd_{0.02}}$. The best fit parameters are summarized in Table 2. The axial space groups with molecular $C_4$ axes co-parallel facilitate single crystal EPR measurements on doped single crystals of $\mathbf{1Y_{0.98}Gd_{0.02}}$ and $\mathbf{2Y_{0.98}Gd_{0.02}}$. These data confirm the validity of the parametrizations, the angular dependence of the resonance lines being well reproduced for various crystal rotations (Fig. 8c and d).

As expected, the *g*-tensors of both compounds are essentially isotropic, and highly comparable. The second and fourth order axial Stevens parameters, $B_2^0$ and $B_4^0$, are remarkably similar between the two different salts, the variation being no more than 6%. The value of $B_6^0$ varies significantly between the two salts, but in both cases, the value is very small, and the effect of this term in the Hamiltonian therefore minimal. The determined value of the real fourth order off-diagonal Stevens parameter $B_4^{+4}$ is identical for $\mathbf{1Y_{0.98}Gd_{0.02}}$ and $\mathbf{2Y_{0.98}Gd_{0.02}}$, but two orders of magnitude smaller than the parameter value of the axial parameter of the equivalent order, and consequently the contribution of the term in the Hamiltonian (1) associated with the $B_4^{+4}$ parameter should be considered small. Rather, the main off-diagonal components of the crystal field are parametrized by the real and imaginary sixth order off-diagonal parameters $B_6^{+4}$ (real) and $B_6^{-4}$ (imaginary). The determined absolute values of these parameters are larger for $\mathbf{1Y_{0.98}Gd_{0.02}}$ over $\mathbf{2Y_{0.98}Gd_{0.02}}$ by factors of 8 and 1.7, respectively. This unambiguously demonstrates the higher symmetry of the **2Ln** compounds, the approximation to the axial $D_{4d}$ point group symmetry being significantly better in these salts compared to the **1Ln** systems. The parameter values determined from the best fits to the parallel mode spectra (red traces in Fig. 8a and b) agree well with those derived from the perpendicular mode data.

The chelation of the lanthanide centres by the metalloligands combined with the high crystallographic symmetry of the salts, places the filled $5d_{z^2}$ orbital of platinum along the four-fold axis with radial extension towards the lanthanide ion. In order to assess the possible role of this occupied orbital in defining the environment of the gadolinium(III) ion, similar powder X-band EPR measurements on doped samples were carried out for **1Gd′** and **2Gd′**. If important, the reduced radial extension of $4d_{z^2}$ orbital of palladium should lead to an alteration of the axial zero-field splitting parameters. The room temperature spectra of the palladium-based complexes $\mathbf{1Y_{0.98}Gd_{0.02}}'$ and $\mathbf{2Y_{0.98}Gd_{0.02}}'$ recorded with the microwave polarization either perpendicular or parallel to the applied magnetic field are given in the lower panels of Fig. 8a and b.

The visual inspection of the spectra clearly demonstrates the strong influence of the group 10 metal ion, the total width of the spectra of the palladium derivatives being less than half of that of the platinum analogues. The best fits of the perpendicular mode spectra to the Hamiltonian (1) nicely reproduce the data as shown by the green traces in the lower panels of Fig. 8a and b. The fit parameters are summarized in Table 2. As the spectra of $\mathbf{1Y_{0.98}Gd_{0.02}}'$ and $\mathbf{2Y_{0.98}Gd_{0.02}}'$ are less rich in detail than those of $\mathbf{1Y_{0.98}Gd_{0.02}}$ and $\mathbf{2Y_{0.98}Gd_{0.02}}$, the parameter values are determined with slightly lower fidelity. In the case of $\mathbf{1Y_{0.98}Gd_{0.02}}'$, the sixth order off-diagonal parameters could not be reliably determined, and consequently the associated terms were excluded from the fit. A fit to the parallel mode spectrum (red trace in Fig. 8a) agrees well with that to the perpendicular mode data for $\mathbf{1Y_{0.98}Gd_{0.02}}'$, but as for the platinum derivatives, the parameters from the parallel mode fitting come with significant uncertainties.

From the best fits, the main origin of the difference between the platinum and palladium derivatives is found to be the value of the second order axial zero-field splitting parameter, $B_2^0$. For $\mathbf{1Y_{0.98}Gd_{0.02}}'$ the determined value is only 27% of the value determined for $\mathbf{1Y_{0.98}Gd_{0.02}}$, while it for $\mathbf{2Y_{0.98}Gd_{0.02}}'$ is 35% of that found for $\mathbf{2Y_{0.98}Gd_{0.02}}$. While the effect is less pronounced for the fourth order axial parameter $B_4^0$, its value decreases consistently upon exchanging platinum with palladium. As for the platinum derivatives, the term associated with the $B_6^0$ parameter is found to be relatively unimportant for $\mathbf{1Y_{0.98}Gd_{0.02}}'$ and $\mathbf{2Y_{0.98}Gd_{0.02}}'$. These findings strongly indicate a significant interaction between the gadolinium centre and the group 10 metal, suggesting a coordination number of ten, rather than the intuitively assigned eight. Such donation of electron density from Pt(II) to a proximate Lewis acid, *i.e.* the Ln(III) ion, was recently evidenced in the heterobimetallic lantern complexes based on the alkaline earth metals using

Table 2 EPR fit parameters derived from the best fits to the Hamiltonian (1) of the perpendicular mode spectra of the gadolinium powder samples at 2% molar concentration in the respective yttrium hosts. The off-diagonal sixth order terms could not be reliably included in the fit for $\mathbf{1Y_{0.98}Gd_{0.02}}'$

| | $\mathbf{1Y_{0.98}Gd_{0.02}}$ | $\mathbf{2Y_{0.98}Gd_{0.02}}$ | $\mathbf{1Y_{0.98}Gd_{0.02}}'$ | $\mathbf{2Y_{0.98}Gd_{0.02}}'$ |
|---|---|---|---|---|
| $g_\parallel$ | 1.9865(3) | 1.9880(2) | 1.979(1) | 1.984(1) |
| $g_\perp$ | 1.98552(4) | 1.98690(7) | 1.9862(8) | 1.9843(1) |
| $B_2^0/\mathrm{cm}^{-1}$ | $3.2378(5) \times 10^{-2}$ | $3.0553(5) \times 10^{-2}$ | $8.8(1) \times 10^{-3}$ | $1.071(4) \times 10^{-2}$ |
| $B_4^0/\mathrm{cm}^{-1}$ | $-2.605(4) \times 10^{-4}$ | $-2.480(2) \times 10^{-4}$ | $-2.0(1) \times 10^{-4}$ | $-2.04(3) \times 10^{-4}$ |
| $B_6^0/\mathrm{cm}^{-1}$ | $-2.8(7) \times 10^{-8}$ | $4(2) \times 10^{-8}$ | $-1(6) \times 10^{-7}$ | $-5(5) \times 10^{-7}$ |
| $B_4^{+4}/\mathrm{cm}^{-1}$ | $1.4(5) \times 10^{-6}$ | $1.4(2) \times 10^{-6}$ | $1.9(3) \times 10^{-5}$ | $6(6) \times 10^{-6}$ |
| $B_6^{+4}/\mathrm{cm}^{-1}$ | $1.62(5) \times 10^{-6}$ | $2.0(3) \times 10^{-7}$ | N/A | $-1.3(7) \times 10^{-6}$ |
| $B_6^{-4}/\mathrm{cm}^{-1}$ | $-6.1(2) \times 10^{-7}$ | $3.6(3) \times 10^{-7}$ | N/A | $-2(3) \times 10^{-7}$ |

$^{195}$Pt NMR, thereby demonstrating the Lewis-basic behaviour of the platinum centre.[39] The minimization of the off-diagonal terms in the Hamiltonian (1) is again found upon going from $\mathbf{1Y_{0.98}Gd_{0.02}}'$ to the higher symmetry $\mathbf{2Y_{0.98}Gd_{0.02}}'$ species. Albeit a direct comparison is hampered by our failure in determining the sixth order off-diagonal parameters for $\mathbf{1Y_{0.98}Gd_{0.02}}'$, we note that the values of $B_4^{+4}$ and $B_6^{-4}$ for $\mathbf{2Y_{0.98}Gd_{0.02}}'$ are found to be equal to zero within error, supporting the notion that the point group symmetry in the $\mathbf{2Ln}'$ compounds is $D_{4d}$ to a very good approximation.

## Conclusions

In summary, we have demonstrated how homoleptic thioacetate complexes of divalent group 10 metal ions can be used as chelating metalloligands in the design of tetragonal complexes of the trivalent lanthanides. Through packing effects with counter cations compatible with four-fold symmetry, the point group symmetry at the lanthanide site in the monoanionic bis metalloligand complexes can be varied between effective $C_4$ in the $[NEt_4]^+$ salts and the higher symmetry $D_{4d}$ in the $[PPh_4]^+$ salts. This symmetry difference deduced from structural analysis is unequivocally confirmed by detailed electron paramagnetic resonance spectroscopy on the gadolinium derivatives. These EPR studies furthermore demonstrate a significant interaction between the filled $nd_{z^2}$ orbital of the platinum metal and the gadolinium ion, supporting a Lewis-basic nature of the platinum(II) centre. Upon going from the $4d_{z^2}$ orbital of palladium to the radially more extended $5d_{z^2}$ orbital of platinum, the leading axial zero-field splitting parameter of $Gd^{3+}$ quadruples, providing strong evidence for a coordination number of ten rather than eight as otherwise assumed from structural analysis. The fact that the platinum metal can be varied renders this class of lanthanide complexes highly tuneable; not only can the point group symmetry at the lanthanide site be altered, so can the ratio between axial and equatorial components of the crystal field. This unprecedented tunability of chemically otherwise unaltered complexes makes this new family of compounds ideal test subjects for studies of the subtleties governing lanthanide magnetism. The in-detail magnetic investigations of selected members of the series are currently being undertaken, and the results will be communicated in the near future.

## Acknowledgements

LHD acknowledges support from NSF-CCT EMT 08-517.

## Notes and references

1 M. Evangelisti, O. Roubeau, E. Palacios, A. Camón, T. N. Hooper, E. K. Brechin and J. J. Alonso, *Angew. Chem., Int. Ed.*, 2011, **50**, 6606–6609.
2 G. Lorusso, J. W. Sharples, E. Palacios, O. Roubeau, E. K. Brechin, R. Sessoli, A. Rossin, F. Tuna, E. J. L. McInnes, D. Collison and M. Evangelisti, *Adv. Mater.*, 2013, **25**, 4653–4656.
3 K. S. Pedersen, G. Lorusso, J. J. Morales, T. Weyhermüller, S. Piligkos, S. K. Singh, D. Larsen, M. Schau-Magnussen, G. Rajaraman, M. Evangelisti and J. Bendix, *Angew. Chem., Int. Ed.*, 2014, **53**, 2394–2397.
4 R. Sessoli, *Angew. Chem., Int. Ed.*, 2012, **51**, 43–45.
5 L. Sorace, C. Benelli and D. Gatteschi, *Chem. Soc. Rev.*, 2011, **40**, 3092–3104.
6 D. N. Woodruff, R. E. P. Winpenny and R. A. Layfield, *Chem. Rev.*, 2013, **113**, 5110–5148.
7 H. L. Feltham and S. Brooker, *Coord. Chem. Rev.*, 2014, **276**, 1–33.
8 S. T. Liddle and J. van Slageren, *Chem. Soc. Rev.*, 2015, **44**, 6655–6669.
9 S.-D. Jiang, B.-W. Wang, G. Su, Z.-M. Wang and S. Gao, *Angew. Chem., Int. Ed.*, 2010, **49**, 7448–7451.
10 N. Ishikawa, M. Sugita, T. Ishikawa, S. Koshihara and Y. Kaizu, *J. Am. Chem. Soc.*, 2003, **125**, 8694–8695.
11 S.-D. Jiang, B.-W. Wang, H.-L. Sun, Z.-M. Wang and S. Gao, *J. Am. Chem. Soc.*, 2011, **133**, 4730–4733.
12 K. R. Meihaus and J. R. Long, *J. Am. Chem. Soc.*, 2013, **135**, 17952–17957.
13 S. Demir, J. M. Zadrozny and J. R. Long, *Chem.–Eur. J.*, 2014, **20**, 9524–9529.
14 M. Gregson, N. F. Chilton, A.-M. Ariciu, F. Tuna, I. F. Crowe, W. Lewis, A. J. Blake, D. Collison, E. J. L. McInnes, R. E. P. Winpenny and S. T. Liddle, *Chem. Sci.*, 2016, **7**, 155–165.
15 Y.-C. Chen, J.-L. Liu, L. Ungur, J. Liu, Q.-W. Li, L.-F. Wang, Z.-P. Ni, L. F. Chibotaru, X.-M. Chen and M.-L. Tong, *J. Am. Chem. Soc.*, 2016, **138**, 2829–2837.
16 C. B. P. Finn, R. Orbach and W. P. Wolf, *Proc. Phys. Soc., London*, 1961, **77**, 261–268.
17 A. Abragam and B. Bleaney, *Electron Paramagnetic Resonance of Transition Ions*, Oxford University Press, Oxford, U.K., 1970.
18 J. D. Rinehart and J. R. Long, *Chem. Sci.*, 2011, **2**, 2078–2085.
19 A. Watanabe, A. Yamashita, M. Nakano, T. Yamamura and T. Kajiwara, *Chem.–Eur. J.*, 2011, **17**, 7428–7432.
20 R. J. Blagg, L. Ungur, F. Tuna, J. Speak, P. Comar, D. Collison, W. Wernsdorfer, E. J. L. McInnes, L. F. Chibotaru and R. E. P. Winpenny, *Nat. Chem.*, 2013, **5**, 673–678.
21 Y.-N. Guo, L. Ungur, G. E. Granroth, A. K. Powell, C. Wu, S. E. Nagler, J. Tang, L. F. Chibotaru and D. Cui, *Sci. Rep.*, 2014, **4**, 5471.
22 J. J. Baldoví, S. Cardona-Serra, J. M. Clemente-Juan, E. Coronado, A. Gaita-Ariño and A. Palii, *Inorg. Chem.*, 2012, **51**, 12565–12574.
23 M. Shiddiq, D. Komijani, Y. Duan, A. Gaita-Ariño, E. Coronado and S. Hill, *Nature*, 2016, **531**, 348–351.
24 K. S. Pedersen, A.-M. Ariciu, S. McAdams, H. Weihe, J. Bendix, F. Tuna and S. Piligkos, *J. Am. Chem. Soc.*, 2016, **138**, 5801–5804.
25 D. C. Bradley, J. S. Ghotra and F. A. Hart, *J. Chem. Soc., Chem. Commun.*, 1972, 349–350.
26 P. G. Eller, D. C. Bradley, M. B. Hursthouse and D. W. Meek, *Coord. Chem. Rev.*, 1977, **24**, 1–95.

 

27 W. J. Evans, D. K. Drummond, H. Zhang and J. L. Atwood, *Inorg. Chem.*, 1988, **27**, 575–579.
28 P. Zhang, L. Zhang, C. Wang, S. Xue, S.-Y. Lin and J. Tang, *J. Am. Chem. Soc.*, 2014, **136**, 4484–4487.
29 A. J. Brown, D. Pinkowicz, M. R. Saber and K. R. Dunbar, *Angew. Chem., Int. Ed.*, 2015, **54**, 5864–5868.
30 N. F. Chilton, C. A. P. Goodwin, D. P. Mills and R. E. P. Winpenny, *Chem. Commun.*, 2015, **51**, 101–103.
31 P. V. Bernhardt, B. M. Flanagan and M. J. Riley, *Aust. J. Chem.*, 2000, **53**, 229–231.
32 P. V. Bernhardt, B. M. Flanagan and M. J. Riley, *Aust. J. Chem.*, 2001, **54**, 229–232.
33 S. Mizukami, H. Houjou, M. Kanesato and K. Hiratani, *Chem.–Eur. J.*, 2003, **9**, 1521–1528.
34 K. S. Pedersen, L. Ungur, M. Sigrist, A. Sundt, M. Schau-Magnussen, V. Vieru, H. Mutka, S. Rols, H. Weihe, O. Waldmann, L. F. Chibotaru, J. Bendix and J. Dreiser, *Chem. Sci.*, 2014, **5**, 1650–1660.
35 C. Piguet, A. F. Williams, G. Bernardinelli and J.-C. G. Bünzli, *Inorg. Chem.*, 1993, **32**, 4139–4149.
36 N. Koike, H. Uekusa, Y. Ohashi, C. Harnoode, F. Kitamura, T. Ohsaka and K. Tokuda, *Inorg. Chem.*, 1996, **35**, 5798–5804.
37 C. Apostolidis, J. Rebizant, B. Kanellakopulos, R. von Ammon, E. Dornberger, J. Müller, B. Powietzka and B. Nuber, *Polyhedron*, 1997, **16**, 1057–1068.
38 K. R. Meihaus, S. G. Minasian, W. W. Lukens, S. A. Kozimor, D. K. Shuh, T. Tyliszczak and J. R. Long, *J. Am. Chem. Soc.*, 2014, **136**, 6056–6068.
39 F. G. Baddour, A. S. Hyre, J. L. Guillet, D. Pascual, J. M. Lopez-de-Luzuriaga, T. M. Alam, J. W. Bacon and L. H. Doerrer, *Inorg. Chem.*, 2017, **56**, 452–469.
40 E. W. Dahl, F. G. Baddour, S. R. Fiedler, W. A. Hoffert, M. P. Shores, G. T. Yee, J.-P. Djukic, J. W. Bacon, A. L. Rheingold and L. H. Doerrer, *Chem. Sci.*, 2012, **3**, 602–609.
41 F. G. Baddour, S. R. Fiedler, M. P. Shores, J. A. Golen, A. L. Rheingold and L. H. Doerrer, *Inorg. Chem.*, 2013, **52**, 4926–4933.
42 F. G. Baddour, S. R. Fiedler, M. P. Shores, J. W. Bacon, J. A. Golen, A. L. Rheingold and L. H. Doerrer, *Inorg. Chem.*, 2013, **52**, 13562–13575.
43 J. L. Guillet, I. Bhowmick, M. P. Shores, C. J. A. Daley, M. Gembicky, J. A. Golen, A. L. Rheingold and L. H. Doerrer, *Inorg. Chem.*, 2016, **55**, 8099–8109.
44 T. Kanda, M. Ibi, K. Mochizuki and S. Kato, *Chem. Lett.*, 1998, 957–958.
45 L. Tian and J. J. Vittal, *Cryst. Growth Des.*, 2006, **6**, 822–824.
46 J. C. Trombe, A. Gleizes and J. Galy, *Inorg. Chim. Acta*, 1984, **87**, 129–141.
47 M. Siebold, A. Kelling, U. Schilde and P. Strauch, *Z. Naturforsch., B: J. Chem. Sci.*, 2005, **60**, 1149–1157.
48 M. Siebold, M. Korabik, U. Schilde, J. Mrozinski and P. Strauch, *Chem. Pap.*, 2008, **62**, 487–495.
49 G.-F. Xu, P. Gamez, J. Tang, R. Clérac, Y.-N. Guo and Y. Guo, *Inorg. Chem.*, 2012, **513**, 5693–5698.
50 M. A. AlDamen, S. Cardona-Serra, J. M. Clemente-Juan, E. Coronado, A. Gaita-Ariño, C. Martí-Gastaldo, F. Luis and O. Montero, *Inorg. Chem.*, 2009, **48**, 3467–3479.
51 O. Kahn, *Molecular Magnetism*, Wiley-VCH, New York, 1993.
52 S. Ghosh, S. Datta, L. Friend, S. Cardona-Serra, A. Gaita-Ariño, E. Coronado and S. Hill, *Dalton Trans.*, 2012, **41**, 13697–13704.
53 J. Krzystek and J. Telser, *Dalton Trans.*, 2016, **45**, 16751–16763.
54 L. Sorace and D. Gatteschi, in *Lanthanides and Actinides in Molecular Magnetism*, WILEY-VCH Verlag GmbH & Co. KGaA, 2015, pp. 1–25.